Kinetic Studies of the Oxidation of Dimethyl Ether and Its Chain Reaction with Cl_2

M. Matti Maricq,* Joseph J. Szente, and John D. Hybl†

Research Laboratory, Ford Motor Company, P.O. Box 2053, Drop 3083, Dearborn, Michigan 48121

Received: March 17, 1997; In Final Form: May 6, 1997[⊗]

The reaction between dimethyl ether radicals and molecular oxygen proceeds along two distinct pathways at temperatures between 230 and 350 K. Above about 100 Torr total pressure the peroxy radical, $CH_3OCH_2O_2$, is predominantly formed. As the pressure is reduced, a channel leading to the formation of OH and two formaldehyde molecules becomes progressively more important. Real time kinetic measurements of these reactions are made using time-resolved UV spectroscopy to monitor CH_3OCH_2 loss and $CH_3OCH_2O_2$ formation along with transient IR absorption to probe formaldehyde production. The OH radicals are identified via their UV spectrum. The reaction can be described via a modified Lindemann mechanism using the three parameters $k_{ro2,\infty}$, $k_{ro2,0}$, and $k_{prod,0}$, which represent the high- and low-pressure limits of the O_2 addition reaction and the low-pressure limit of the OH/formaldehyde channel. At 295 K they have values of $(1.1 \pm 0.1) \times 10^{-11}$ cm^3 s^{-1}, $(2.6 \pm 0.9) \times 10^{-29}$ cm^6 s^{-1}, and $(6 \pm 2) \times 10^{-12}$ cm^3 s^{-1}, respectively. At $P_{tot} = \sim$120 Torr the reaction exhibits a negative temperature dependence with $k_{r+o2} = (3.1^{+1.0}_{-0.8}) \times 10^{-12}\ e^{(326\pm80)/T}$ cm^3 s^{-1}. Experiments in the absence of oxygen were performed to investigate the CH_3OCH_2-mediated chain reaction between chlorine and dimethyl ether. Analysis of time-resolved UV spectra reveals rate constants of $k_{r+cl2} = (1.8^{+0.7}_{-0.5}) \times 10^{-11}\ e^{(360\pm120)/T}$ cm^3 s^{-1} and $k_{r+r} = (1.8^{+0.6}_{-0.5}) \times 10^{-11}\ e^{(200\pm100)/T}$ cm^3 s^{-1}, respectively, for the chain propagation reaction between CH_3OCH_2 and molecular chlorine and for the chain-terminating recombination reaction.

Introduction

The oxidation of dimethyl ether is of interest on two counts: From the atmospheric chemistry perspective it is the simplest representative of the class of ether compounds, some of which (e.g. methyl *tert*-butyl ether, MTBE) find use as automotive fuel additives.[1] From the standpoint of combustion chemistry, dimethyl ether has been advanced, due to its high cetane number and low soot production, as an alternative, low-emissions, diesel fuel.[2] An interesting property of dimethyl ether is that its combustion is readily initiated by compression ignition; that is, it has a high cetane number. In contrast to other ethers the cetane number is very high (CN > 55), comparable, or even superior, to conventional diesel fuel.[2] Concomitantly, whereas other ethers, such as MTBE, find application as octane enhancers,[1] dimethyl ether exhibits a very low octane number and would function poorly in this regard.

A possible explanation for dimethyl ether's compression ignition propensity lies in its oxidation chemistry. Previous product studies of the chlorine atom initiated low-temperature oxidation of dimethyl ether revealed a dependence on total pressure;[3] as the pressure is lowered, formaldehyde is produced at the expense of CH_3OCHO. This observation was explained by postulating two channels for the reaction between methoxymethyl radicals and oxygen,

$$CH_3OCH_2 + O_2 + M \rightarrow CH_3OCH_2O_2 + M \qquad (1a)$$

$$CH_3OCH_2 + O_2 \rightarrow 2\ CH_2O + OH \qquad (1b)$$

the conventional oxygen addition reaction along with a bimolecular channel, both of which presumably proceed through an excited reaction complex, $CH_3OCH_2O_2$*.

Verification of OH radical formation would have important implications with respect to the compression ignition of dimethyl ether, since this radical is an important reactive intermediate in the combustion process. Alkyl radical oxidation reactions are usually dominated by processes leading to the much less reactive hydroperoxy and organic peroxy radicals, until the temperature becomes sufficiently high to sustain combustion. If hydroxyl radicals are formed directly at lower temperature during the initial steps of dimethyl ether oxidation, they would attack the fuel in a catalytic fashion, providing a plausible mechanism for the facile initiation of combustion.

The time-resolved observations of OH and CH_2O reported here furnish direct evidence for the proposed rearrangement/dissociation channel of the reaction between CH_3OCH_2 and molecular oxygen. Kinetic data for this reaction are determined not only by following the loss of CH_3OCH_2 with time but also by measuring the appearance of $CH_3OCH_2O_2$ and CH_2O, producing a consistent picture of this reaction. Temperature and pressure dependent rate constants are presented for this reaction as well as for the chain reaction between CH_3OCH_2 and Cl_2 and for the CH_3OCH_2 recombination reaction. These data are compared to previous measurements on this system.

Experimental Section

The kinetics of the reactions of CH_3OCH_2 with itself, Cl_2, and O_2 were interrogated using time-resolved UV spectroscopy[4] and transient infrared absorption,[5] both of which have been previously described. The former technique was used to probe the intermediate CH_3OCH_2, OH, and $CH_3OCH_2O_2$ radicals formed in these reactions as well as the loss of Cl_2. Transient infrared absorption was used to monitor formaldehyde generation.

Time-resolved UV spectra are collected using a gated diode array spectrometer. Broad-band UV light from either a D_2 or Xe lamp propagates through the cell in a direction opposite to the photolysis beam, is dispersed by a monochromator, and impinges the array detector, which is gated to measure the

* Author to whom correspondence is addressed.
† Present address: Department of Chemistry, University of Colorado, Boulder, CO 80309.
⊗ Abstract published in *Advance ACS Abstracts,* June 15, 1997.

S1089-5639(97)00966-3 CCC: $14.00

transmitted light intensity at specified times 4−300 μs after the photolysis pulse. At each delay time the recorded absorbance consists of contributions from each absorbing species weighted by its UV absorption spectrum and concentration; thus,

$$\mathrm{Abs}(\lambda,t) = \sum_i l\sigma_i(\lambda)\, C_i(t) \qquad (2)$$

These spectra are subsequently deconvolved, using independently measured absorption cross sections for each species, to provided the time variation in the concentration of each absorbing species over the course of the reaction. In the present experiments these species include CH_3OCH_2, $CH_3OCH_2O_2$, Cl_2, CH_3OCH_2Cl, and CH_3OCH_3; however, the last two molecules exhibit nearly identical spectra over the 190−350 nm region investigated, and only their combined concentration change can be followed (the spectra are illustrated in Figure 1).

Formaldehyde formation is monitored via vibration−rotation lines of the ν_2 carbonyl stretch mode at 1729 cm^{-1}. Radiation from a lead salt diode laser propagates through the cell and is focused onto a HgCdTe detector with a 0.3 μs response time. The detector responds only to changes in IR light intensity; thus, the absolute intensity is added to the transient response prior to the use of Beer's law to extract the formaldehyde concentration via

$$[CH_2O]_t = \frac{1}{\sigma_{CH_2O} l}\ln\left(\frac{I_0 + I(t)}{I_0}\right) \qquad (3)$$

where l is the pathlength, σ_{CH_2O} is the IR absorption cross section, and I_0 is the diode laser intensity. The absorption strength is measured at the temperature and pressure of each experiment and for each vibration−rotation line used as a probe by introducing a known amount of formaldehyde into the reaction cell. The formaldehyde is obtained by heating paraformaldehyde, and its concentration is confirmed by FT-IR analysis.

The oxidation and chain reaction studies of dimethyl ether were performed by combining laser flash photolysis to initiate the radical chemistry and the above described time-resolved spectroscopic techniques to monitor the important chemical species. Two sources of CH_3OCH_2 were utilized: 351 nm photolysis of Cl_2 followed by hydrogen abstraction from dimethyl ether,

$$Cl + CH_3OCH_3 \rightarrow CH_3OCH_2 + HCl \qquad (4)$$

and 193 nm photolysis of phosgene into 2Cl + CO followed by reaction 4. Because the rate constant for reaction 4 is large,[6] $k_4 = 1.9 \times 10^{-10}$ cm^3 s^{-1}, only a small amount of dimethyl ether (0.5 Torr) is required to convert the chlorine atoms produced by photolysis into methoxymethyl radicals on a short time scale (<0.5 μs) compared to the subsequent reactions of CH_3OCH_2. However, when Cl_2 (∼0.2 Torr) is used as the radical precursor, the situation is somewhat more complicated than for phosgene. The chain reaction

$$CH_3OCH_2 + Cl_2 \rightarrow CH_3OCH_2Cl + Cl \qquad (5)$$

implies that a steady state population of chlorine atoms relative to CH_3OCH_2, equal to $k_5[Cl_2]/k_4[CH_3OCH_3]$, will be quickly established following chlorine photolysis. To ensure that this ratio is small, i.e., that the radical population consists predominantly of CH_3OCH_2, necessitates considerably higher dimethyl ether concentrations (∼5 Torr).

A second difficulty incurred with the use of Cl_2 photolysis to initiate the radical chemistry stems from our observation that dimethyl ether reacts spontaneously with molecular chlorine. To what extent this reaction is heterogeneous remains uncertain; however, the impact in our experiments was that only about 85% of the chlorine added to the reaction mixture actually reached the cell. This reaction is quenched by the addition of even a small amount of oxygen, implying that it likely proceeds via the intermediate CH_3OCH_2 radical. Due to quenching by O_2, the spontaneous reaction affected only the measurements of the $CH_3OCH_2 + Cl_2$ and $CH_3OCH_2 + CH_3OCH_2$ reaction rate constants. The means of accounting for this interference is discussed in the Results section below.

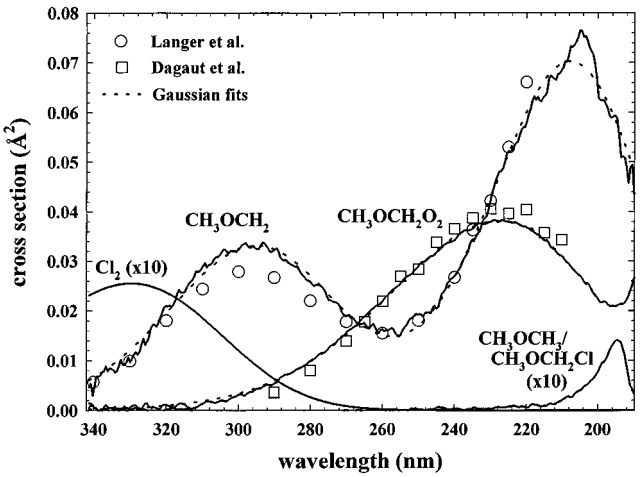

Figure 1. UV spectra of CH_3OCH_2 and $CH_3OCH_2O_2$. These are compared to previously reported cross sections by Langer et al.[9] and Dagaut et al.,[10] respectively. The dotted traces represent best fits of the spectra to a Gaussian line shape. Spectra of Cl_2 and the CH_3OCH_3/CH_3OCH_2Cl composite are also illustrated for comparison.

The use of $COCl_2$ as a chlorine atom source introduces two complications into the experiments. First, 193 nm light causes some O_2 dissociation and the subsequent formation of ozone, a strong UV absorber. At the O_2 concentrations employed in the present experiments, this problem occurred predominantly outside the cell, but within the photolysis and probe beam paths. The extent of ozone formation was measured independently and its contribution subtracted from the individual time-resolved spectra. Second, the 193 nm radiation dissociates some of the dimethyl ether reactant into CH_3 and CH_3O. This is readily observed by the appearance of a sharp absorption feature at 216 nm characteristic of the methyl radical. Quantification of this absorption indicates that the formation of these dissociation products is limited to <15% of the Cl atom production under our experimental conditions. The effects of the methyl and methoxy radicals on our kinetics measurements are considered below.

The experiments were carried out using premixed gas mixtures, either $Cl_2/CH_3OCH_3/N_2$ or $COCl_2/CH_3OCH_3/N_2$, each with or without added O_2, that are slowly flowed through a thermostated cylindrical cell that is 51 cm long and 3.2 cm in diameter. A 15 ns, 200−400 mJ, pulse from an excimer laser operating at 193 nm for $COCl_2$, or at 351 nm for Cl_2, passes longitudinally through the central portion of the cell (∼1.5 cm diameter) of which the central 0.8 cm diameter region is probed. A Neslab ULT 80dd recirculating chiller maintains the cell temperature and preconditions the gas mixture over a range of 215−360 K. Tylan flow controllers are employed to regulate the individual gas flows, with the exception of Cl_2, which is adjusted by a needle valve.

Results

A. UV Spectra. The UV spectrum of the CH_3OCH_2 radical was measured in three ways: photolysis of phosgene in a

$COCl_2/CH_3OCH_3/N_2$ gas mixture, photolysis of Cl_2 in a $Cl_2/CH_3OCH_3/N_2$ mixture, and photolysis of Cl_2 in a $Cl_2/CH_3OCH_3/O_2/N_2$ mixture. The spectra were measured at a variety of times shortly after photolysis (2−10 μs) and extrapolated back to time zero. The initial concentration of chlorine atoms produced by the photolysis pulse was ascertained by substituting ethane for dimethyl ether, ensuring that oxygen was present in the gas mixture, and recording the absorption intensity of the ethylperoxy radicals that were formed.[7] Ethylperoxy radicals are rapidly formed, but only slowly removed via their self-reaction, and, thus, afford a convenient calibration standard.

The absorption intensities recorded from phosgene photolysis and from Cl_2 photolysis with oxygen present were in quantitative agreement over the 215−350 nm range. Information cannot be obtained below 215 nm for phosgene photolysis owing to the 193 nm optics used to introduce the photolysis beam into the cell. The absorption intensity measured using the Cl_2 precursor in the absence of oxygen was about 15% smaller than from the other two types of measurements, but otherwise exhibited the same wavelength dependence. Consistent with this observation, the 330 nm absorption of Cl_2 was found to fall by about 15% when dimethyl ether is introduced into the gas stream. As stated above, this occurs due to a (possibly heterogeneous) reaction between CH_3OCH_3 and Cl_2 that depletes a small fraction of the chlorine prior to its reaching the cell.

The CH_3OCH_2 spectrum determined from the three types of measurements is presented in Figure 1. It exhibits two absorption bands: one with a maximum at 295 nm and a second band having a maximum intensity at 204 nm. These two bands can be conveniently represented as the sum of two Gaussian profiles

$$\sigma(\lambda) = \sum_i \sigma_i \exp(-\alpha_i[\ln(\lambda_{i,\max}/\lambda)]^2) \qquad (6)$$

with $\sigma_1 = 7.0 \times 10^{-18}$ cm^2, $a_1 = 47.8$, $\lambda_{1,\max} = 208$ nm, $\sigma_2 = 3.3 \times 10^{-18}$ cm^2, $a_2 = 81.4$, and $\lambda_{2,\max} = 295$ nm. As apparent from Figure 1, this expression gives a very good representation of the CH_3OCH_2 spectrum, except for a small region near the peak of the short wavelength band, which the fitted expression underestimates by about 10%.

The $CH_3OCH_2O_2$ spectrum was measured by the same method as just described for the methoxymethyl radical, except that a high concentration of O_2, ∼10 Torr, was employed in the reaction mixture to convert rapidly the CH_3OCH_2 radicals to peroxy radicals. The spectrum was measured as a function of O_2 pressure, total pressure, and time following photolysis. The O_2 and total pressures were increased until no change was noted upon further increase in either quantity; this occurs for $[O_2] > 5$ Torr and $P_{tot} > 100$ Torr. The latter condition is consistent with the observation that the $CH_3OCH_2 + O_2$ reaction channel leading to formaldehyde represents less than about 5% of the overall reaction above this pressure.

The $CH_3OCH_2O_2$ spectra obtained from 193 nm photolysis of phosgene and 351 nm photolysis of Cl_2 are essentially identical. The spectrum, illustrated in Figure 1, is put on an absolute intensity scale by calibration against the absorption by ethylperoxy radicals. It consists of a broad absorption feature, as is typical of peroxy radicals, with the hint of a shorter wavelength band beginning below 200 nm. As evident from Figure 1, a Gaussian profile provides an excellent representation of the longer wavelength band of the $CH_3OCH_2O_2$ spectrum (for $\lambda > 200$ nm), being virtually indistinguishable from the experimental trace. In this case, $\sigma = 3.8 \times 10^{-18}$ cm^2, $a = 31.7$, and $\lambda_{\max} = 228$ nm.

TABLE 1: Mechanism for the $Cl_2-CH_3OCH_3$ Chain Reaction

reaction[a]	rate constant (k)
4. $Cl + CH_3OCH_3 \rightarrow CH_3OCH_2 + HCl$	1.9×10^{-10} cm^3 s^{-1} [6]
5. $CH_3OCH_2 + Cl_2 \rightarrow CH_3OCH_2Cl + Cl$	$1.8 \times 10^{-11}e^{360/T}$ cm^3 s^{-1} [b]
7. $CH_3OCH_2 + CH_3OCH_2 \rightarrow (CH_3OCH_2)_2$	$1.8 \times 10^{-11}e^{200/T}$ cm^3 s^{-1} [b]
8. $CH_3OCH_2 + Cl \rightarrow$ products	$(0-2) \times 10^{-10}$ cm^3 s^{-1}

When using 193 nm photolysis of $COCl_2$, the reactions below were added to the model,[c] with the initial CH_3 and CH_3O concentrations set equal to 15% of $[Cl]_0$

$CH_3 + CH_3 \rightarrow C_2H_6$	6×10^{-11} cm^3 s^{-1}
$CH_3 + CH_3O \rightarrow$ products	4×10^{-11} cm^3 s^{-1}
$CH_3O + CH_3O \rightarrow$ products	3×10^{-11} cm^3 s^{-1}
$CH_3OCH_2 + CH_3 \rightarrow$ products	$(0-6) \times 10^{-11}$ cm^3 s^{-1}
$CH_3OCH_2 + CH_3O \rightarrow$ products	$(0-6) \times 10^{-11}$ cm^3 s^{-1}

[a] Reaction numbers correspond to those used in the text. [b] Measured in the present study. [c] Rate constants are taken from the NIST database.[8] Those for the reactions involving CH_3OCH_2 are varied over the indicated range.

The errors in the CH_3OCH_2 and $CH_3OCH_2O_2$ absorption cross sections are estimated to be somewhat less than 10%. The ethylperoxy calibration spectrum is accurate to about 5%. An additional 5% is allowed for small changes that might have occurred when ethane and O_2 are substituted for dimethyl ether in the gas mixture and for the short extrapolation of the absorption to zero time.

The methoxymethyl and methoxymethylperoxy spectra discussed above are used to extract concentrations of the corresponding species from time-resolved spectra of the reaction mixture. The actual experimental spectra, and not the Gaussian fits, are used for this purpose. Besides these, two additional terms are included in the deconvolution represented by eq 2: the first accounts for the loss of molecular chlorine and the second is a composite term that accounts for the loss of dimethyl ether and the corresponding formation of CH_3OCH_2Cl. As previously stated, the latter two compounds absorb weakly in the region below about 210 nm, but with spectra that are not readily distinguishable. This term is included to preclude a systematic bias on the determination of the CH_3OCH_2, $CH_3OCH_2O_2$, and Cl_2 concentrations; however, its contribution to the overall absorption is not used in the subsequent kinetic analysis.

B. Chain Reaction. Photolysis of Cl_2 in the presence of CH_3OCH_3 initiates a chain reaction represented by reactions 4 and 5. Figure 2 illustrates how the absorbance of the reaction mixture changes over time. At time zero, the two absorption bands characteristic of the methoxymethyl radical are evident. As time progresses, the intensities of these features decrease owing to the loss of this radical; however, the changes in intensity are not uniform over wavelength. At long times, a short wavelength feature appears at about 200 nm. Furthermore, the absorption decreases below zero in the 330 nm region.

These spectral changes are consistent with a reaction mechanism (see Table 1) that consists of the chain propagation reactions as well as the termination reaction

$$CH_3OCH_2 + CH_3OCH_2 \rightarrow (CH_3OCH_2)_2 \qquad (7)$$

Reaction 7 accounts for the decreases in intensity of the bands at 295 and 204 nm. In principle, the reaction between methoxymethyl radicals and chlorine atoms,

$$CH_3OCH_2 + Cl \rightarrow \text{products} \qquad (8)$$

also contributes, but under the present experimental conditions this reaction, as well as the chlorine atom recombination

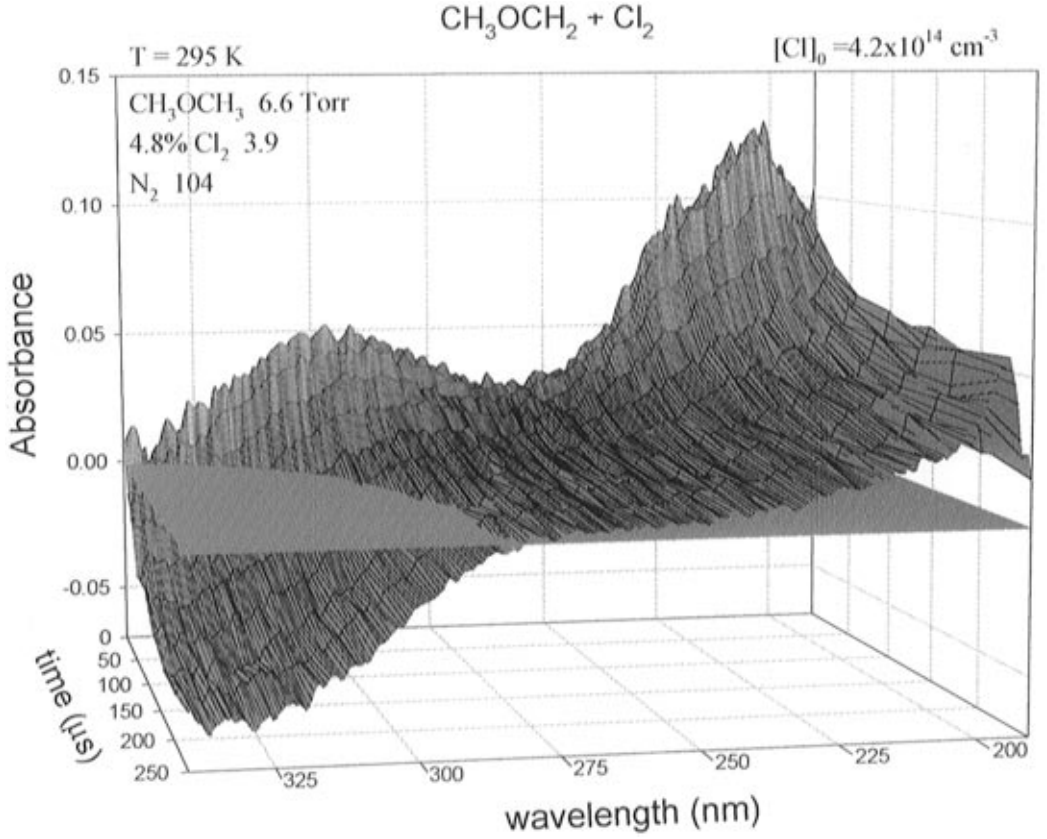

Figure 2. Absorbance−wavelength−time surface for the Cl-mediated chain reaction of dimethyl ether and chlorine.

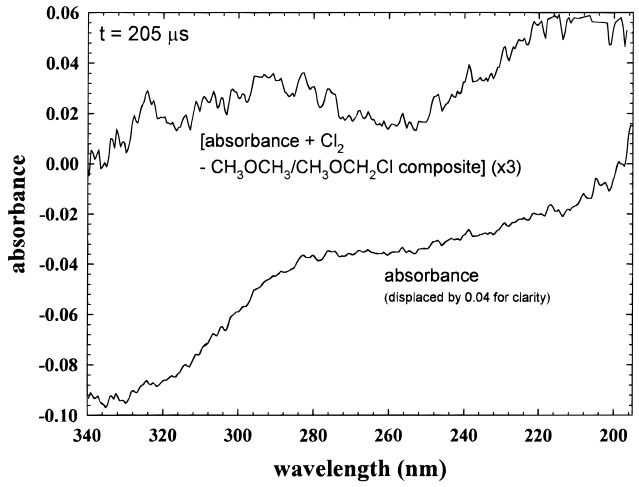

Figure 3. Illustration of the deconvolution procedure for the 205 μs time slice of Figure 2. Shown are the absorbance of the reaction mixture and the methoxymethyl contribution obtained after subtracting out the best fit contributions made by the Cl_2 loss and the CH_3OCH_2/CH_3OCH_2Cl composite.

reaction, is unimportant since the steady state radical population fulfills $[CH_3OCH_2]_{ss} >> [Cl]_{ss}$. Prior to its removal, however, each methoxymethyl radical cycles through reactions 4 and 5 roughly 20 times on average. This removes on the order of 10^{16} cm^{-3} chlorine molecules, explaining the negative absorbance that develops at 330 nm. The chain also converts an equal number of CH_3OCH_3 molecules into CH_3OCH_2Cl. Each of these two species has an absorption band with an onset in the vicinity of 200 nm, but the chloride has the stronger absorption; thus the short wavelength feature appears at long times.

Fitting the time-resolved absorbances to reference spectra of CH_3OCH_2, Cl_2, and the CH_3OCH_3/CH_3OCH_2Cl composite

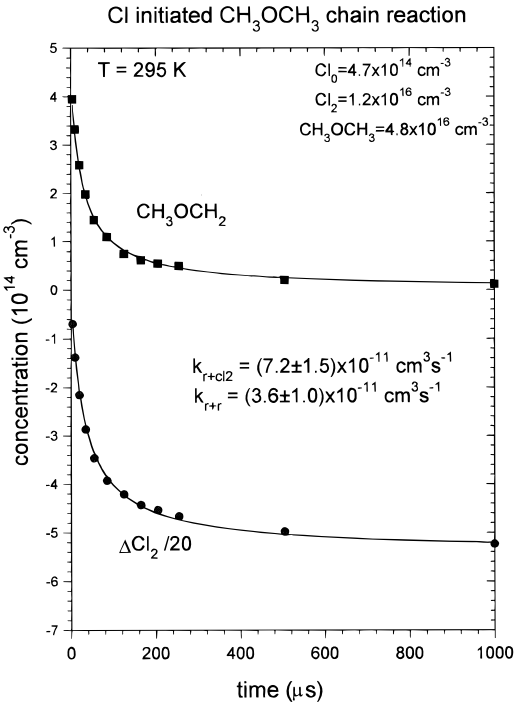

Figure 4. Methoxymethyl and molecular chlorine concentration versus time profiles obtained by deconvolution of the time-resolved spectra. The solid lines show best fits of the model in Table 1 to the data.

absorption provides time-varying concentration profiles for the methoxymethyl radical and chlorine. Figure 3 demonstrates the deconvolution procedure, and Figure 4 illustrates the resulting concentration profiles. The Cl_2 concentrations have been scaled down by a factor of 20 for purposes of illustration and in order that they do not inordinately weight the fitting of the data to the reaction model.

TABLE 2: Measured Rate Constants for the Reactions $CH_3OCH_2 + CH_3OCH_2$ and $CH_3OCH_2 + Cl_2$

temp (K)	radical source[a] source; conc (10^{16} cm^{-3})	conditions CH_3OCH_3 (10^{16} cm^{-3})	conditions P_{tot} (Torr)	conditions $[Cl]_0$ (10^{14} cm^{-3})	results[b] k_{r+r} (10^{-11} cm^3 s^{-1})	results[b] k_{r+cl2} (10^{-11} cm^3 s^{-1})
220	Cl_2; 0.80	28	112	4.6	4.1 ± 0.8	9.3 ± 1.5
231	Cl_2; 1.2	27	413	5.3	4.8 ± 1.0	8.1 ± 1.4
260	Cl_2; 0.95	24	25	5.1	3.9 ± 0.8	7.0 ± 1.3
295	Cl_2; 0.64	5.0	112	3.6	3.5 ± 0.6	6.4 ± 0.9
295	Cl_2; 0.61	22	116	3.6	3.3 ± 0.7	6.4 ± 1.0
295	Cl_2; 0.85	21	114	6.8	3.4 ± 0.6	5.5 ± 0.8
295	Cl_2; 0.70	20	112	1.6	3.4 ± 0.7	6.2 ± 0.8
295	Cl_2; 1.2	4.8	113	4.6	3.6 ± 1.0	7.2 ± 1.5
295	$COCl_2$; 0.25	1.6	122	5.2	3.6 ± 0.6	
325	$COCl_2$; 0.25	1.5	451	5.4	3.7 ± 0.6	
327	Cl_2; 0.53	19	120	3.7	3.0 ± 0.6	5.0 ± 0.9
357	Cl_2; 0.86	17	58	4.4	3.2 ± 0.6	4.8 ± 0.9

[a] Listed concentrations are determined by measurements of gas flows. Due to the reaction between Cl_2 and CH_3OCH_3, actual chlorine concentrations in the cell were approximately 85% of the tabulated value. [b] Error bars are $\pm 2\sigma$ and include systematic uncertainties.

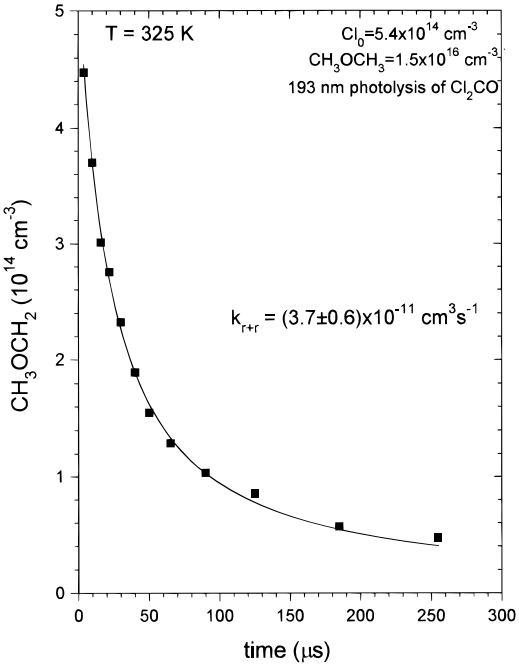

Figure 5. Decay of CH_3OCH_2 produced by the photolysis of $COCl_2$ in the presence of dimethyl ether. The solid line shows the fit of the data by the model.

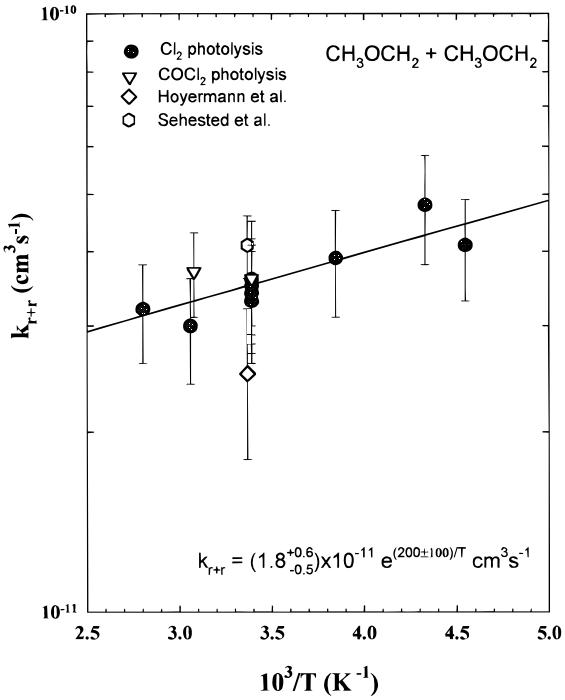

Figure 6. Temperature dependence of the CH_3OCH_2 self-reaction rate constant. Also shown are the values reported by Hoyermann et al.[12] and Sehested et al.[11]

The concentration versus time data are fit to the reaction model of Table 1 treating k_{r+r} and k_{r+cl2}, the rate constants for reactions 7 and 5, respectively, as adjustable parameters. Examples of the quality of fit are provided by the solid lines in Figure 4. The rate constants are collected, along with the pertinent experimental conditions, in Table 2. The errors are $\pm 2\sigma$ and include both the data scatter and systematic uncertainties. In the case of k_{r+cl2} the latter are dominated by uncertainties in the optical cross sections of CH_3OCH_2 and Cl_2 and in the initial radical concentration, as measured by the ethylperoxy calibration method. A 10% uncertainty in $\sigma_{ch3och2}$ introduces a ~8% error, a 5% uncertainty in σ_{cl2} contributes 8%, and a 10% uncertainty in $[Cl]_0$ contributes about 5% to the overall error in k_{r+cl2}, whereas uncertainties in the values of k_4 and k_8 have a negligible impact. Combining these statistically with a 5% fitting error leads to 2σ error bars in the vicinity of ±16%. The errors in k_{r+r} also derive primarily from uncertainties in $\sigma_{ch3och2}$, σ_{cl2}, and $[Cl]_0$. In this case the fit is more sensitive to the CH_3OCH_2 cross section, which contributes a 15% error, and the initial radical concentration, which contributes a 10% error. Combined with a 10% error from data scatter, the net error in k_{r+r} is approximately ±20%.

Additional measurements of the CH_3OCH_2 self-reaction rate constant were made using the photolysis of $COCl_2$ in the presence of dimethyl ether. After removing the contribution made by ozone formed outside the reaction cell, the time-resolved spectra reveal the characteristic methoxymethyl absorption bands, which decay in time without changes in the wavelength dependence. This is consistent with the second-order removal of CH_3OCH_2 into a form having at most a minor optical absorption in the 200−340 nm range. The time dependence of $[CH_3OCH_2]$ at 325 K derived from these spectra is provided by Figure 5.

The analysis of the data when using the $COCl_2$ precursor differs somewhat from the above discussion. In the absence of Cl_2 the chain reaction plays no role; thus, reaction 5 is omitted from the model. However, additional chemistry, listed in Table 1, is included to account for reactions of the CH_3 and CH_3O radicals that are produced from the 193 nm photolysis of CH_3OCH_3 (kinetic data for these reactions are obtained from the NIST database[8]). Their rates of reaction with CH_3OCH_2 are unknown and, thus, introduce an uncertainty into the determi-

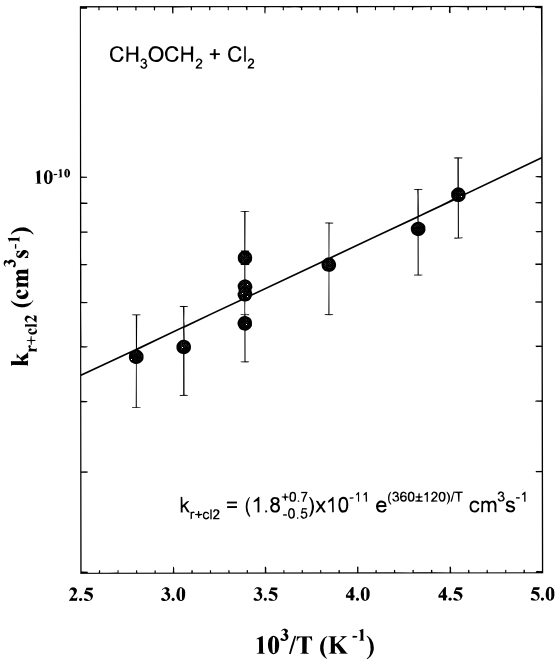

Figure 7. Temperature dependence of the $CH_3OCH_2 + Cl_2$ reaction rate constant.

nation of $k_{r+r.}$ Fortunately this uncertainty is small since the initial CH_3 and CH_3O concentrations are approximately 8 times less than $[Cl]_0$. Thus, variation of the rate constants over the range $(0-6) \times 10^{-11}$ cm^3 s^{-1}, a range reasonable for radical−radical reactions between alkyl and alkoxy radicals, affects the best fit values of k_{r+r} by about ±7%. The rate constants derived from this modified model, listed in Table 1, are in excellent agreement with those derived from Cl_2 photolysis. In addition to the uncertainties introduced by dimethyl ether dissociation, there are 10% errors from data scatter and from the uncertainty in $\sigma_{ch3och2}$ that result in a statistically combined 2σ error of ∼±17%.

The variations with temperature of the rate constants for the CH_3OCH_2 self-reaction and its reaction with chlorine are presented in Figures 6 and 7, respectively. Both exhibit a negative temperature dependence, which is mildly surprising in the case of the radical−molecule reaction. Expressed in the Arrhenius form, the self reaction rate constant is given by $k_{r+r} = (1.8^{+0.6}_{-0.5}) \times 10^{-11} e^{(200\pm100)/T}$ cm^3 s^{-1}, whereas the rate constant for the reaction with molecular chlorine is $k_{r+cl2} = (1.8^{+0.7}_{-0.5}) \times 10^{-11} e^{(360\pm120)/T}$ cm^3 s^{-1}.

C. Reaction of CH_3OCH_2 with O_2. *i. High Pressure: The Peroxy Radical Channel.* Adding oxygen to a $Cl_2/CH_3OCH_3/N_2$ gas mixture dramatically changes the shape of the absorption−wavelength−time surface recorded following Cl_2 photolysis, as is evident from comparing Figures 8 and 2. In both cases, the absorption at early time is characteristic of the methoxymethyl radical; however, the decay below zero of the absorption at 330 nm is less pronounced when oxygen is present, and more importantly, a new absorption feature peaking at about 225 nm appears rapidly, within 50 μs of the photolysis pulse. This new feature matches the $CH_3OCH_2O_2$ spectrum illustrated in Figure 1.

Qualitatively these changes in the optical absorption of the reaction mixture are what one would expect from the addition of O_2 to the methoxymethyl radical to yield the corresponding peroxy radical. Fits of the time-resolved spectra to reference spectra of CH_3OCH_2, $CH_3OCH_2O_2$, Cl_2, and the CH_3OCH_3/CH_3OCH_2Cl composite yield the concentration versus time profiles illustrated in Figure 9. The decay of the methoxymethyl radical is accompanied by a rapid rise in $CH_3OCH_2O_2$ concentration. There is still some loss of Cl_2; however, it is diminished when oxygen is present because the $CH_3OCH_2 + O_2$ reaction

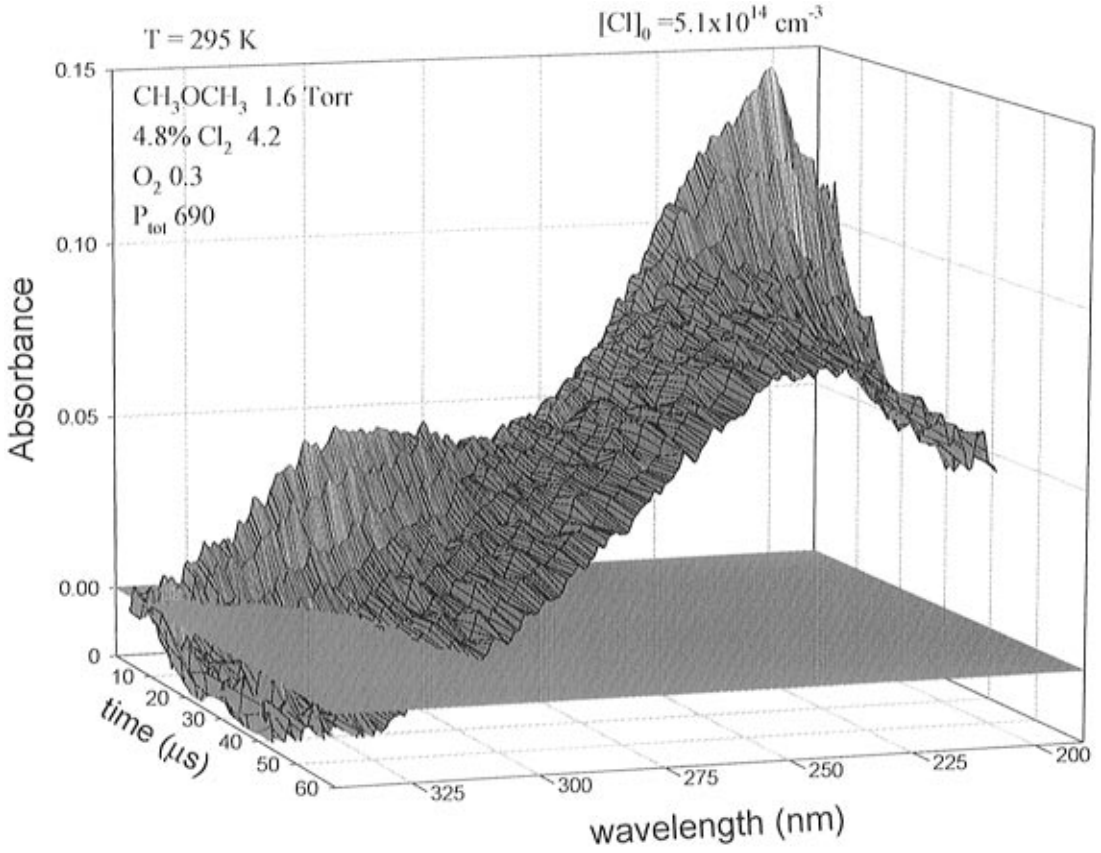

Figure 8. Absorbance−wavelength−time surface for the Cl-initiated oxidation of dimethyl ether.

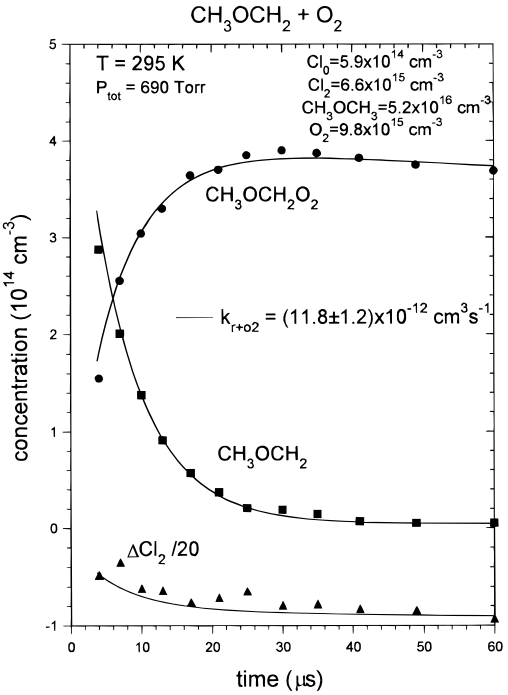

Figure 9. Methoxymethyl, methoxymethylperoxy, and molecular chlorine concentration versus time profiles obtained by deconvolution of time-resolved spectra obtained using Cl_2 photolysis. The solid lines show best fits of the model in Table 3 to the data.

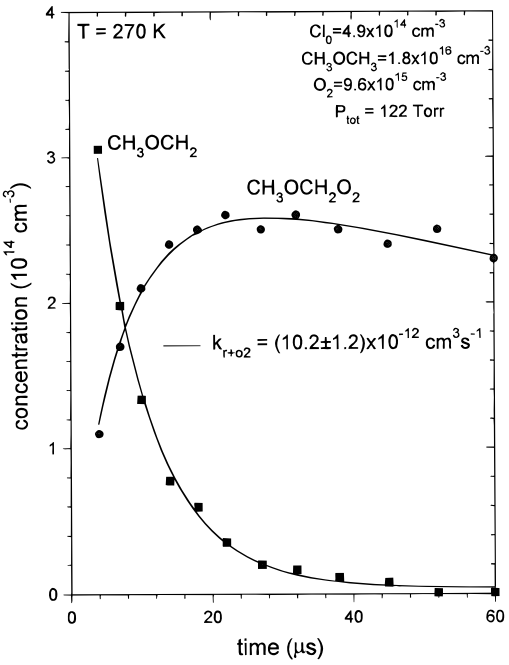

Figure 10. Methoxymethyl and methoxymethylperoxy concentration versus time profiles obtained by deconvolution of time-resolved spectra obtained using phosgene photolysis. The solid lines show best fits of the model in Table 3 to the data.

acts as an additional chain termination step. The results remain unchanged when the CH_3OCH_2 radical is generated by $COCl_2$ photolysis, as shown by Figure 10, except for the obvious fact that there is no accompanying Cl_2 loss.

The apparent simplicity of the above discussion belies a number of underlying complexities inherent in this system. The principal one, the pressure dependence of the $CH_3OCH_2 + O_2$ reaction, is discussed below; here we consider the mechanism assuming that only the peroxy radical is formed, which is appropriate for total pressures greater than about 100 Torr.[3] Even under these conditions, however, simply augmenting the chain reaction of Table 1 with the reaction

$$CH_3OCH_2 + O_2 + M \rightarrow CH_3OCH_2O_2 + M \qquad (1a)$$

is not sufficient to permit satisfactory fits of the data; the model underestimates the rate of methoxymethyl radical decay and overestimates the quantity of peroxy radicals formed. Adding the cross reaction

$$CH_3OCH_2 + CH_3OCH_2O_2 \rightarrow \text{products} \qquad (9)$$

corrects these deficiencies and leads to excellent fits of the data, treating k_{r+o2} and k_9 as adjustable parameters. The values obtained for k_9 lie in the range $(2-8) \times 10^{-11}$ cm^3 s^{-1}; those for k_{r+o2} are listed in Table 3.

The fits of the concentration versus time profiles shown by the solid lines in Figures 9 and 10 are obtained using the more complete reaction mechanism provided in Table 4 (including a contribution by channel 1b of <6% at $P_{tot} > 100$ Torr), although the additional chemistry only slightly affects the fits. Aside from the above reactions this model includes the peroxy radical self-reaction and the ensuing regeneration

TABLE 3: Measured Rate Constants for the $CH_3OCH_2 + O_2$ Reaction

temp (K)	radical source source; conc (10^{16} cm^{-3})	conditions CH_3OCH_3 (10^{16} cm^{-3})	conditions O_2 (10^{16} cm^{-3})	conditions P_{tot} (Torr)	conditions $[Cl]_0$ (10^{14} cm^{-3})	results k_{r+O2} (10^{-12} cm^3 s^{-1})
			versus T at ~120 Torr			
220	Cl_2; 0.82	26	1.0	111	4.6	12.9 ± 1.7
229	$COCl_2$; 1.1	2.1	1.1	118	5.3	12.4 ± 2.0
252	Cl_2; 0.77	8.8	0.77	108	4.9	13.1 ± 1.8
270	$COCl_2$; 0.89	1.8	0.96	120	4.9	10.2 ± 1.2
295	$COCl_2$; 0.84	1.6	0.47	119	5.6	9.3 ± 1.4
295	Cl_2; 0.64	4.8	0.78	110	4.4	9.2 ± 1.2
295	$COCl_2$; 0.86	1.6	0.89	122	5.7	9.5 ± 1.1
295	$COCl_2$; 0.84	1.6	1.8	122	5.4	9.4 ± 1.2
295	$COCl_2$; 1.7	1.6	1.7	125	6.0	8.9 ± 1.2
355	Cl_2; 0.59	6.4	0.6	110	3.7	7.6 ± 1.0
			versus P_{tot} at 295 K			
295	Cl_2;0.58	5.2	0.49	5.4	3.2	8.5 ± 1.5
295	Cl_2;0.71	5.2	1.4	6.5	5.6	7.1 ± 1.2
295	$COCl_2$; 0.87	1.6	0.87	53	5.2	9.0 ± 1.1
295	$COCl_2$; 0.86	1.5	0.85	206	5.0	10.0 ± 1.3
295	$COCl_2$; 0.89	1.6	0.81	442	5.6	10.8 ± 1.3
295	Cl_2; 0.70	8.0	0.75	480	4.4	11.6 ± 1.8
295	Cl_2; 0.70	5.2	0.98	690	5.9	11.8 ± 1.2

TABLE 4: Mechanism for the $CH_3OCH_2 + O_2$ Reaction

	reaction[a]	rate constant (k)
	Principal	
4.	$Cl + CH_3OCH_3 \rightarrow CH_3OCH_2 + HCl$	1.9×10^{-10} cm^3 s^{-1} [6]
1a.	$CH_3OCH_2 + O_2 + M \rightarrow CH_3OCH_2O_2 + M$	see text
1b.	$CH_3OCH_2 + O_2 \rightarrow 2CH_2O + OH$	see text
	Radical−Radical	
10a.	$CH_3OCH_2O_2 + CH_3OCH_2O_2 \rightarrow 2CH_3OCH_2O + O_2$	$(3-6) \times 10^{-12}$ cm^3 s^{-1}
10b.	$CH_3OCH_2O_2 + CH_3OCH_2O_2 \rightarrow CH_3OCHO + CH_3OCH_2OH + O_2$	$(1-2) \times 10^{-12}$ cm^3 s^{-1}
7.	$CH_3OCH_2 + CH_3OCH_2 \rightarrow (CH_3OCH_2)_2$	$1.8 \times 10^{-11}e^{200/T}$ cm^3 s^{-1} [b]
9.	$CH_3OCH_2 + CH_3OCH_2O_2 \rightarrow$ products	$(2-8) \times 10^{-11}$ cm^3 s^{-1}
8.	$CH_3OCH_2 + Cl \rightarrow$ products	$(0-2) \times 10^{-10}$ cm^3 s^{-1}
	Chain	
13.	$OH + CH_3OCH_3 \rightarrow CH_3OCH_2 + H_2O$	$6.7 \times 10^{-12}e^{-300/T}$ cm^3 s^{-1} [8]
11.	$CH_3OCH_2O \rightarrow CH_3OCHO + H$	$0-\infty$ s^{-1}
12.	$H + CH_3OCH_2O_2 \rightarrow CH_3OCH_2O + OH$	$(0-1) \times 10^{-10}$ cm^3 s^{-1}
	$H + Cl_2 \rightarrow Cl + HCl$	$1.4 \times 10^{-10}e^{-590/T}$ cm^3 s^{-1} [8]
5.	$CH_3OCH_2 + Cl_2 \rightarrow CH_3OCH_2Cl + Cl$	$1.8 \times 10^{-11}e^{360/T}$ cm^3 s^{-1} [b]

[a] Reaction numbers correspond to those used in the text. [b] Measured in the present study.

of CH_3OCH_2 radicals. The latter occurs via

$$CH_3OCH_2O_2 + CH_3OCH_2O_2 \rightarrow 2CH_3OCH_2O + O_2 \quad (10a)$$

$$CH_3OCH_2O \rightarrow CH_3OCHO + H \quad (11)$$

in which one channel of the $CH_3OCH_2O_2$ peroxy radical self-reaction yields the corresponding alkoxy radical, which subsequently ejects a hydrogen atom. The competing reaction between CH_3OCH_2O and O_2 is too slow at the oxygen concentrations of this study to be of consequence. Hydrogen atoms formed by reaction 11 can add O_2, which is slow under the present conditions because of the low O_2 concentrations employed, react with dimethyl ether, which is slow compared to the Cl_2 reaction, or react with Cl_2 to regenerate chlorine atoms. Potentially they could also react with peroxy radicals,

$$CH_3OCH_2O_2 + H \rightarrow CH_3OCH_2O + OH \quad (12)$$

with the interesting consequence of producing one methoxymethyl radical, from OH attack of dimethyl ether, and regenerating the hydrogen atom via reaction 11. Although provided here for completeness and although important for understanding the subsequent chemistry of the $CH_3OCH_2O_2$ radicals, reactions 10−12 have only a minor influence on the decay of the methoxymethyl radical and on the determination of k_{r+o2}.

The temperature dependence of the $CH_3OCH_2 + O_2$ reaction was investigated at a total pressure in the vicinity of 120 Torr. The results are listed in Table 3 and illustrated by Figure 11. A fit of the data to the Arrhenius form yields $k_{r+o2}(120\ \text{Torr}) = (3.1^{+1.0}_{-0.8}) \times 10^{-12}e^{(326\pm80)/T}$ cm^3 s^{-1}. The reaction exhibits a negative temperature dependence, as expected for an addition reaction.

ii. Low Pressure: The Hydroxyl Radical Channel. The data shown in Figures 8−11 and described above were recorded at pressures greater than 100 Torr. Another level of complexity arises as the total pressure is lowered below this level. The product study of Sehested et al.[3] observed an increase in formaldehyde formation, from about 15% at 100 Torr to 120% at 5 Torr, which they attributed to the competing reaction channel

$$CH_3OCH_2 + O_2 \rightarrow 2CH_2O + OH \quad (1b)$$

A direct observation of this channel is presented in Figure 12, which shows the absorbance of a $Cl_2/CH_3OCH_3/O_2$ gas mixture at 5.5 Torr total pressure 8 μs after photolysis. The upper trace reveals the $v'' = 0 \rightarrow v' = 0$ and $v'' = 0 \rightarrow v' = 1$ bands of the

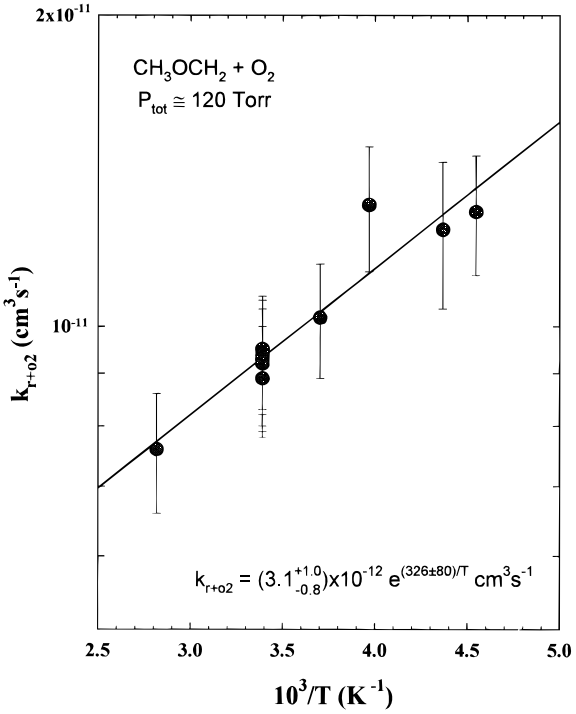

Figure 11. Temperature dependence of the reaction between CH_3OCH_2 and O_2 at 120 Torr total pressure.

X $^2\Pi \rightarrow$ A $^2\Sigma^+$ transition of the hydroxyl radical at 308.6 and 282.5 nm, respectively, which are superimposed on the long wavelength tail of the $CH_3OCH_2O_2$ spectrum. This is confirmed by the OH spectrum shown in the lower trace, which is obtained by the photolysis of F_2 in the presence of water vapor via the reaction

$$F + H_2O \rightarrow OH + HF$$

By calibrating the OH absorption intensity at the spectral resolution of our spectrometer against the absorption by ethylperoxy radicals formed when ethane and O_2 are substituted for water vapor, we find the OH concentration in the upper trace to be 2.8×10^{14} cm^{-3}, a value in good agreement with the reaction mechanism given in Table 4 and discussed below.

Direct observation of channel 1b is also provided by the IR diode laser transient absorption measurements of formaldehyde generation that are presented in Figure 13. The amount of CH_2O formed falls with increasing total pressure such that the branching fraction for channel 1b decreases from $f = 0.45$ at

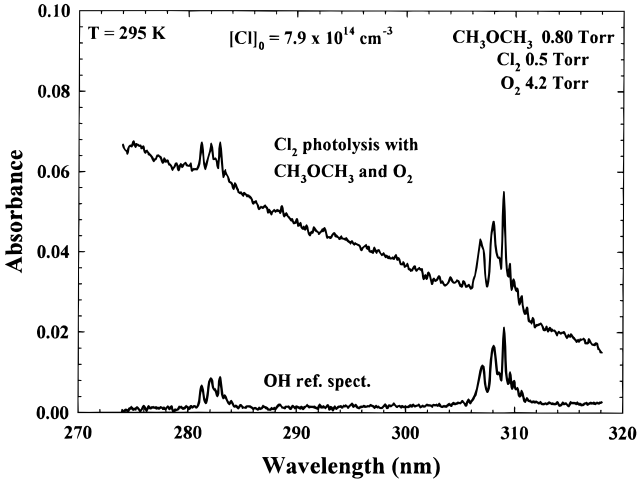

Figure 12. X $^2\Pi \rightarrow$ A $^2\Sigma^+$ transition of the hydroxyl radical formed from the reaction between CH_3OCH_2 and O_2.

$P_{tot} = 5$ Torr to a value of 0.17 at 48 Torr. Similar results are obtained when phosgene, as opposed to chlorine, photolysis is used to initiate the reaction (see Table 5).

Aside from the fact that two competing channels are active below about 100 Torr, the formation of OH further complicates matters. It introduces an additional chain reaction into the overall mechanism since the hydroxyl radical will attack dimethyl ether,

$$OH + CH_3OCH_3 \rightarrow CH_3OCH_2 + H_2O \qquad (13)$$

and regenerate a methoxymethyl radical. This is included in the reaction mechanism of Table 4. Fitting the formaldehyde formation traces to this model, treating k_{r+o2} and f as adjustable parameters and setting $k_9 = 5 \times 10^{-11}$ cm^3 s^{-1}, leads to the smooth line fits of the data shown in Figure 13.

As seen from Table 5, the values of k_{r+o2} obtained from these fits are in the range $(2.8-5.5) \times 10^{-12}$ cm^3 s^{-1}, 2−3 times smaller than the rate constant at $P_{tot} > 100$ Torr. In fact, the rate constants found from formaldehyde formation are smaller by roughly a factor of 2 than those determined at the same total pressure from CH_3OCH_2 loss and $CH_3OCH_2O_2$ formation using time-resolved UV spectroscopy. A plausible explanation for this is as follows. The formation of formaldehyde and the hydroxyl radical via reaction 1b is exothermic by 40 kcal/mol. This excess energy is sufficient to produce vibrationally excited CH_2O molecules. Since the diode laser probes the $v = 0 \rightarrow v = 1$ transition of the ν_2 carbonyl stretch, excited molecules would initially be transparent to the probe. As time progresses and the excited molecules are collisionally relaxed to the ground state, they would contribute to the total IR absorbance. Consequently, the observed rate constant for CH_2O formation, being a convolution of fk_{r+o2} and the vibrational relaxation rate constant, will appear smaller than the true value. This problem should decrease as P_{tot} increases owing to faster relaxation; however, sensitivity also decreases because of line broadening

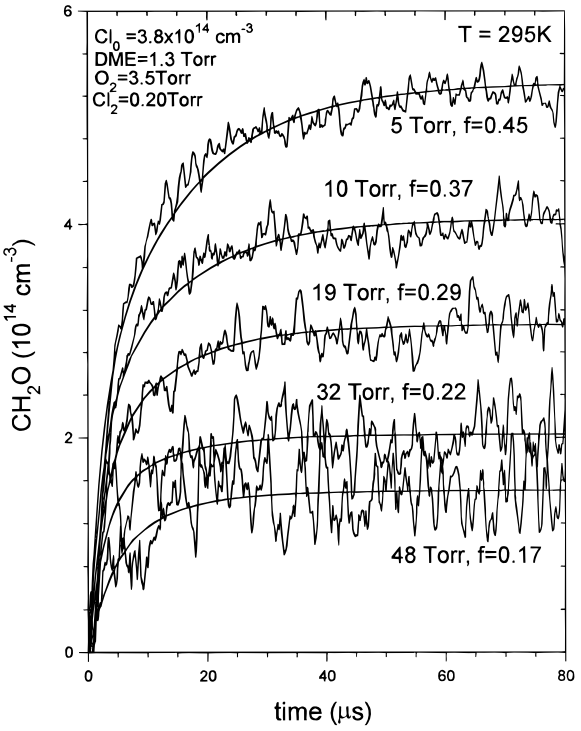

Figure 13. IR diode laser transient absorption measurements of the formaldehyde formed from the $CH_3OCH_2 + O_2$ reaction as a function of total pressure.

TABLE 5: Yield of Channel 1b from Transient CH_2O Measurements

temp (K)	radical source source; conc (10^{16} cm^{-3})	conditions CH_3OCH_3 (10^{16} cm^{-3})	conditions O_2 (10^{16} cm^{-3})	conditions P_{tot} (Torr)	conditions $[Cl]_0$ (10^{14} cm^{-3})	results[a] k_{r+O2} (10^{-12} cm^3 s^{-1})	results[a] f
230	Cl_2; 0.80	5.5	14	4.9	4.9	4.7	0.37
230	Cl_2; 0.80	5.5	14	10.0	4.5	3.6	0.30
230	Cl_2; 0.84	5.5	15	21.0	4.7	2.5	0.22
230	Cl_2; 0.84	5.5	14	34.7	4.9		0.14
295	Cl_2; 0.65	4.3	11	4.9	3.5	3.7	0.46
295	Cl_2; 0.65	4.3	12	10.2	3.8	3.5	0.37
295	Cl_2; 0.65	4.3	11	19.0	4.0	3.1	0.29
295	Cl_2; 0.65	4.3	11	32.0	3.8	3.4	0.22
295	Cl_2; 0.65	4.3	11	47.5	3.9		0.18
295	$COCl_2$; 1.0	4.3	13	6	4.1	2.8	0.50
295	$COCl_2$; 0.85	4.3	11	10.4	4.1	3.0	0.44
295	$COCl_2$; 0.82	4.3	11	24.9	4.6	2.5	0.27
295	$COCl_2$; 0.82	4.3	11	50.1	5.0	1.2	0.19
295	$COCl_2$; 0.88	4.3	12	80.3	5.1		0.13
350	Cl_2; 0.55	3.6	9.4	5	3.2	3.4	0.52
350	Cl_2; 0.55	3.6	9.2	10	2.9	3.0	0.47
350	Cl_2; 0.52	3.6	8.8	20	3.7	3.0	0.38
350	Cl_2; 0.58	3.6	9.9	35	3.8	2.5	0.28
350	Cl_2; 0.58	3.6	9.7	50	3.2	3.3	0.22

[a] The values of k_{r+o2} and f are lower bounds owing to possible vibrational excitation of the CH_2O; see text. f is the branching fraction for reaction 1b.

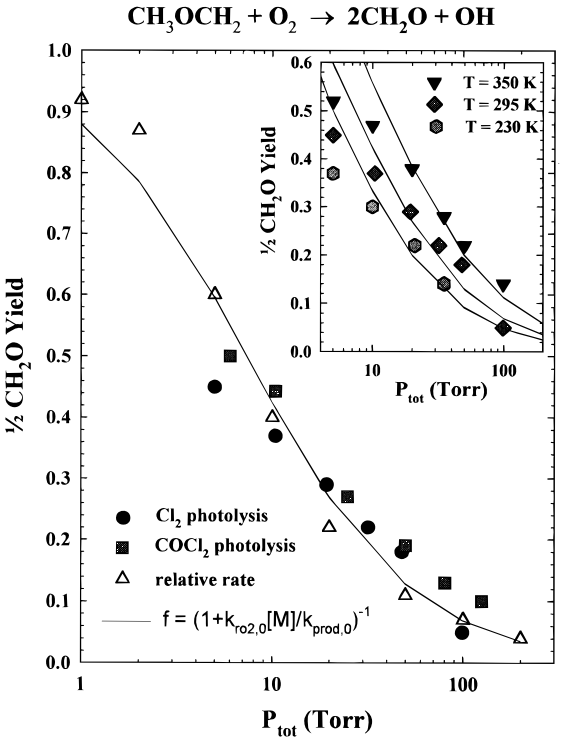

Figure 14. Pressure dependence of the branching fraction for the formaldehyde channel of the $CH_3OCH_2 + O_2$ reaction. Also shown are values from the product study of Sehested et al.[3] The inset shows the variation with temperature of the pressure dependent formaldehyde channel.

whereby the measurement of k_{ro2} becomes less reliable. An example of the extent to which nascent vibrational excitation can mask the true kinetics is provided in a previous paper[5] investigating ethylene formation from the reaction of C_2H_5 and Cl.

By similar arguments, generation of excited formaldehyde by reaction 1b will lead to underestimates of the branching fraction for this channel that depend systematically on the total pressure. Rigorously then, the pressure dependent formaldehyde yields exhibited in Figure 14 and listed in Table 5 would be expected to represent lower limits of the yield. However, as comparison to the product study of Sehested et al.[3] reveals, the limit is quite close to the actual values. This is likely because the branching fraction, which is determined by the level of formaldehyde at relatively long times (80 μs in Figure 13), is less sensitive to vibrational relaxation than k_{r+o2}, which depends predominantly on the shape of the formaldehyde curve at short times (0−20 μs). Close examination of Figure 14 reveals that vibrational excitation may have some effect on the determination of *f*; the CH_2O yield as recorded by transient IR absorption is somewhat smaller than that determined via the product study at the lowest pressure. The inset to Figure 14 compares the pressure dependence of the CH_2O yield at various temperatures. Increasing the temperature at a set total pressure has the effect of promoting formaldehyde formation, channel 1b, relative to peroxy radical formation, channel 1a.

iii. Error Analysis. The quantities of interest in the investigation of the $CH_3OCH_2 + O_2$ reaction kinetics are k_{r+o2} and $f = k_{1b}/k_{r+o2}$ (where $k_{r+o2} \equiv k_{1a} + k_{1b}$), the branching fraction for the formaldehyde channel. For measurements conducted using time-resolved UV absorption, the data were fit to the reaction model of Table 4, with k_{r+o2}, k_9, and k_{10} treated as adjustable parameters. In these cases, the branching fraction was fixed to the value reported in ref 3, because, as discussed above, the present IR measurements of *f* could underestimate it due to vibrational excitation of the nascent CH_2O. The transient IR measurements of formaldehyde were fit to the same model, except that k_{r+o2} and *f* were allowed to vary, whereas k_9 and k_{10} were fixed to the midpoints of their respective ranges, as determined from the fits of the UV data.

For the UV measurements made with $P_{tot} > 100$ Torr, the errors in k_{r+o2} arise predominantly from the fitting error and uncertainties in $\sigma_{ch3och2}$, $\sigma_{ch3och2o2}$, and *f*. The fitting error amounts to about 8% and includes contributions from data scatter and the uncertainty in k_9 (as stated previously, k_{10} has little influence on k_{r+o2}; it affects the decay of RO_2). Uncertainties of 10% in the absolute intensities of the reference UV spectra each contribute roughly 7% to the overall error. Variation of *f* between 0 and 0.1, nearly twice the measured value at 100 Torr, introduces another 5% error into k_{r+o2}. Smaller contributions come from uncertainties of 10% in $[Cl]_0$, 20% in k_{r+r}, and 10% in k_4, which introduce errors of 4%, 1.5%, and 2%, respectively. Combining these errors statistically yields a typical error in k_{r+o2} of ±15%.

The preceding error analysis applies to results obtained using both Cl_2 and $COCl_2$ photolysis. Recall that, with respect to k_{r+r} and k_{r+cl2}, an additional error arises when phosgene is the precursor from the uncertainties introduced by small quantities of CH_3 and CH_3O radicals produced by the 193 nm photolysis of dimethyl ether. The interference by these radicals in the measurement of k_{r+o2} is much smaller, because the loss of the CH_3OCH_2 radical is dominated by its reaction with O_2. Instead, their impact will be on the subsequent chemistry of the RO_2 radical.

Errors in the UV measurements of k_{r+o2} for $P_{tot} < 100$ Torr become progressively larger as the total pressure decreases. Mainly this due to the more complex chemistry inherent at low pressure; partly it is due to loss in signal to noise owing to the reduced levels of peroxy radicals that are formed. By 5 Torr the net error is close to ±20%. In principle the reverse is true for the IR measurements based on formaldehyde formation. Owing to collisional line broadening, the sensitivity of the technique increases as P_{tot} decreases. Unfortunately, vibrational relaxation rates decrease as the pressure is lowered; thus, the increase in sensitivity is offset by the increasing influence of the relaxation process on the rate of formaldehyde appearance. The determinations of *f* suffer the same fate, but to a lesser extent. The best estimate of their accuracy is probably obtained by comparison of our results to those obtained from the product study of Sehested et al.[3]

Discussion

A. UV Spectra. The UV spectrum of the methoxymethyl radical is compared in Figure 1 to previous work by Langer et al.[9] In extrapolating to zero time, small corrections (∼10%) have been made to the spectrum to account for CH_3OCH_2 loss, Cl_2 loss, CH_3OCH_3 loss, and CH_3OCH_2Cl formation. As evident from the figure, there is good agreement between the general features of the two spectra. Both reveal two absorption bands and agree on the wavelength maximum of the longer wavelength band. There is a small discrepancy between the two spectra in that the intensity of the 295 nm band recorded by Langer et al.[9] is roughly 15% smaller than the present measurement, whereas the intensities of the short wavelength bands appear to be in good agreement. This could be due to systematic variability incurred in making single-point intensity measurements that are absent in the present experiments in which the entire spectrum is measured simultaneously.

The $CH_3OCH_2O_2$ spectrum has been recorded previously by Dagaut et al.[10] and Jenkin et al.[6] These determinations are

virtually identical, so only the data of Dagaut et al. are compared in Figure 1 to the present measurements. It is apparent that the spectra are in very good agreement. Both exhibit a broad structureless band peaking at 225 nm, which is typical of peroxy radicals. The work of Jenkin et al.[6] utilized both molecular modulation and pulsed radiolysis to generate methoxymethylperoxy radicals. The shape of the spectrum obtained via the former method exhibited a dependence on the $[O_2]/[Cl_2]$ ratio, which the authors attributed to the H atom ejection in reaction 11 followed by oxygen addition to form HO_2. This radical also absorbs in the UV, at shorter wavelengths than $CH_3OCH_2O_2$, and thus, its presence would alter the observed composite spectrum. In the present study, the O_2 concentration was too low and the time after photolysis too short for enough HO_2 to form to interfere with the $CH_3OCH_2O_2$ spectrum. Most of the previous measurements were made near atmospheric pressure; therefore, effects that the formaldehyde/OH channel of the $CH_3OCH_2 + O_2$ reaction might have on the apparent $CH_3OCH_2O_2$ were avoided.

B. Chain Reaction. The investigation of the Cl-initiated chain reaction between dimethyl ether and chlorine was carried out under conditions such that the radical population following photolysis was dominated by CH_3OCH_2. This introduces two simplifications into the reaction mechanism: first, radical−radical reactions other than the self-reaction of the methoxymethyl radical are of negligible importance and, second, precise knowledge of the rate constant for the $Cl + CH_3OCH_3$ reaction is not necessary. The mechanism is therefore well approximated by two reactions, the self-reaction of CH_3OCH_2 and its reaction with molecular chlorine. By simultaneously fitting the chlorine and methoxymethyl concentration profiles, the rate constants for these two reactions could be determined. Independent verification of the self-reaction rate constant was provided by the experiments utilizing phosgene photolysis to generate CH_3OCH_2, under conditions in which the self reaction represented the dominant reaction of this radical.

The results for k_{r+r} are compared in Figure 6 to previous room-temperature determinations by Sehested et al.[11] and Hoyermann et al.[12] The present rate constants are intermediate to the previous versions and agree with both within the combined error bars. Our measurements show k_{r+r} to be independent of pressure between 25 and 400 Torr. This is consistent with the small difference between the value of k_{r+r} obtained by Hoyermann et al. at 1−4 Torr total pressure versus the value obtained at 1 atm of SF_6 by Sehested et al. The latter authors observed no systematic variation of k_{r+r} with temperature over the 296−523 K range. We find the self-reaction to exhibit a small negative temperature dependence with $k_{r+r} = (1.08^{+0.6}_{-0.5}) \times 10^{-11} e^{(200\pm100)/T}$ cm^3 s^{-1}. This expression exhibits only a 35% change over the temperature extremes of the Sehested et al.[11] study and, thus, may be obscured within their data scatter.

A direct investigation of the $CH_3OCH_2 + Cl_2$ reaction has not, to our knowledge, been previously reported, although the relative rate with respect to O_2 has been measured.[3] Within the scope of our measurements, between 25 and 400 Torr, the reaction appears to be pressure independent, as expected for a bimolecular reaction. We find it to have a negative temperature dependence, given by $k_{r+cl2} = (1.8^{+0.7}_{-0.5}) \times 10^{-11} e^{(360\pm120)/T}$ cm^3 s^{-1}. Negative temperature dependences have been observed before for this type of reaction, e.g., the iso-$C_3H_7 + Cl_2$ reaction.[13]

C. O_2 Reaction. The addition of O_2 to form a peroxy radical is ubiquitous among organic radicals. Above about 100 Torr, the methoxymethyl radical, too, undergoes this pressure dependent reaction. Where this radical differs from others of its type, however, is in its low-pressure behavior, in which a reaction channel forming hydroxyl radicals and formaldehyde becomes important. This reaction was posited by Sehested et al.[3] to explain the increase with decreasing pressure of formaldehyde product from the chlorine-initiated photooxidation of dimethyl ether. It is confirmed here by the direct, time-resolved, observation of both the OH radical and formaldehyde products. However, it was apparently overlooked in the previous low-pressure investigations of the $CH_3OCH_2 + O_2$ reaction by Hoyermann et al.[12] and Masaki et al.[14] Both groups used mass spectrometry to follow the reaction kinetics, yet reported observing only the peroxy radical product. This is perhaps understandable in the work of Masaki et al.,[14] since they employed photoionization by a Xe resonance lamp (8.44 eV), presumably to avoid ionizing the dimethyl ether parent compound (IP 9.96 eV), and, thus, would have missed the formation of formaldehyde (IP 10.88 eV). It is unclear why this channel was not observed by Hoyermann et al.,[12] who utilized electron impact ionization (energy of 10−29 eV).

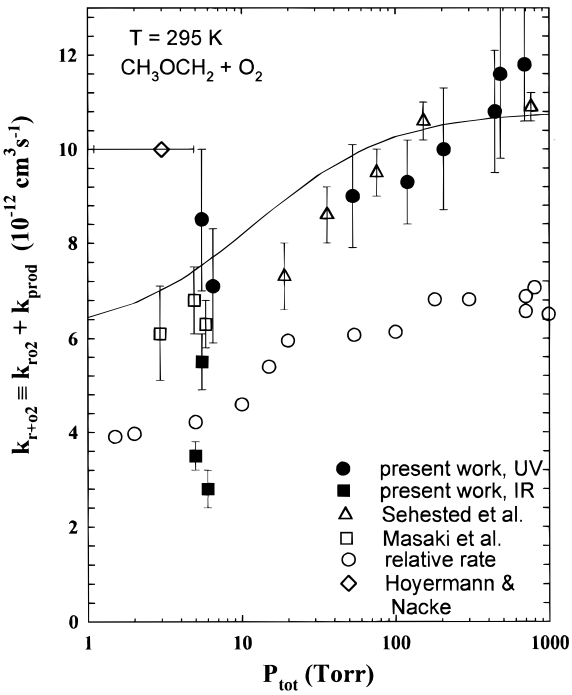

Figure 15. Pressure dependence of the reaction between CH_3OCH_2 and O_2 at 295 K. The present results are compared to previous direct and indirect measurements of k_{r+o2}. The relative rate data of Sehested et al.[3] are placed on an absolute scale using our determination of k_{r+cl2}. The solid line is a fit of our data to the modified Lindemann mechanism, eqs 14−16.

The present measurements of k_{r+o2} at high pressures ($P_{tot} >$ ∼100 Torr) are in very good agreement with the recently reported values of Sehested et al.,[11] as evident from the comparison made in Figure 15 (although it is not clear if they accounted for reaction 9 in their analysis). It is interesting that both sets of rate constants exhibit nearly the same small pressure dependence in spite of the fact that one set utilized a bath gas of N_2 whereas the other employed SF_6. Our UV measurements of k_{r+o2} at low pressure (∼5 Torr) agree well with those of Masaki et al.,[14] but are somewhat smaller than the value reported by Hoyermann et al.[12] However, this may be somewhat fortuitous owing to the omission of channel 1b from the reaction mechanism by the latter groups. In fact, substituting the experimental conditions of Masaki et al.[14] into the model of Table 4 leads to a predicted CH_3OCH_2 loss that mimics an exponential decay, although one that decays to a constant

nonzero offset, with an apparent rate constant comparable to the true value.

Two other sets of measurements shown in Figure 15 deserve comment. First are the values of k_{r+o2} derived from the rate of formaldehyde production. That they are smaller than those from the UV measurements is attributed to vibrational excitation of the nascent CH_2O, which makes a fraction of this product initially transparent to the IR probe. Its subsequent vibrational relaxation causes an apparent formaldehyde appearance rate that is slower than the actual formation rate. Second are rate constants derived from the relative rate determinations[3] of k_{r+o2}/k_{r+cl2} by scaling them with the current measurement of k_{r+cl2}. These values underestimate the kinetically derived values of k_{r+o2} by about 30%. While the agreement between direct and relative rate measurements is reasonably good, it does stretch the combined error bars. The origin of the discrepancy remains uncertain. Because of the good agreement between the various direct determinations of k_{r+o2}, this is an unlikely source of the discrepancy. This leaves the present evaluation of k_{r+cl2} and the relative rate measurement as candidates. Were the discrepancies to arise from k_{r+cl2}, its already large value of 6.2×10^{-11} cm^3 s^{-1}, as compared to other R + Cl_2 reactions, would have to be elevated to about 1×10^{-10} cm^3 s^{-1}. Alternatively, there may exist some, as of yet unknown, subtlety concerning the relative rate experiments.

Assuming that both channels 1a and 1b proceed through an intermediate complex that is either stabilized or dissociates allows, via a Lindemann analysis, the pressure dependence of the reaction to be parametrized according to

$$k_{ro2} \equiv k_{1a} = \frac{k_{ro2,0}[M]}{1 + k_{ro2,0}[M]/k_{ro2,\infty}} \qquad (14)$$

$$k_{prod} \equiv k_{1b} = \frac{k_{prod,0}}{1 + k_{ro2,0}[M]/k_{ro2,\infty}} \qquad (15)$$

where $k_{ro2,0}$ is a three-body rate constant that depends on the nature of the bath gas (here N_2), and $k_{ro2,\infty}$ is the high-pressure limit. A fit of $k_{r+o2} = k_{ro2} + k_{prod}$ to our pressure dependent data in Figure 15 leads to values for $k_{ro2,0}$ and $k_{prod,0}$ of 1.3×10^{-30} cm^6 s^{-1} and 7.8×10^{-12} cm^3 s^{-1}, respectively. However, *f*, the branching fraction for channel 1b, is given by

$$f = \frac{1}{1 + k_{ro2,0}[M]/k_{prod,0}} \qquad (16)$$

and fits to eq 16 of the formaldehyde yield pressure dependence in Figure 14 give $k_{ro2,0}/k_{prod,0} = 4.3 \times 10^{-18}$ cm^3. Clearly, this ratio is incompatible with the individual parameters deduced from the pressure dependence of k_{r+o2} in Figure 15. This problem is resolved by noting that the three-parameter fits of k_{r+o2} to eqs 14 and 15 are insensitive to the choice of $k_{ro2,0}$ and, consequently, that this parameter is essentially indeterminate within the accuracy of the measured rate constants. $k_{prod,0}$ and $k_{ro2,\infty}$, on the other hand, are fit with reasonable accuracy. Therefore, $k_{ro2,0}$ is deduced from fitting the formaldehyde yield to eq 16. At 295 K the results are $k_{ro2,0} = (2.6 \pm 0.9) \times 10^{-29}$ cm^6 s^{-1}, $k_{ro2,\infty} = (11 \pm 1) \times 10^{-12}$ cm^3 s^{-1}, and $k_{prod,0} = (6 \pm 2) \times 10^{-12}$ cm^3 s^{-1}. The solid line in Figure 15 represents the predicted pressure dependence of k_{r+o2} based on these parameters.

Sehested et al.[11] also fit the pressure dependence of the k_{r+o2} rate constant by combining their high-pressure data with the low-pressure rate constants of Masaki et al.[14] Their values of $(11.4 \pm 0.4) \times 10^{-12}$ cm^3 s^{-1} and $(6.0 \pm 0.5) \times 10^{-12}$ cm^3 s^{-1} for $k_{ro2,\infty}$ and $k_{prod,0}$, respectively, are in very good agreement with the present results, with the caveat that the low-pressure rate constants were determined without consideration of reaction 1b. Their value for $k_{ro2,0}$ of $(9.4 \pm 4.2) \times 10^{-30}$ cm^6 s^{-1} is well below our determination; however, it too suffers from the data being insensitive to this parameter. It is clearly too small since a prediction of the formaldehyde yield based on this value for $k_{ro2,0}$ gives $k_{ro2,0}/k_{prod,0} = 1.6 \times 10^{-18}$ cm^3, a value nearly one-third that required to fit the formaldehyde yield in Figure 14.

Including the present work, there are three determinations of the temperature dependence of the $CH_3OCH_2 + O_2$ reaction; however, all three are measured under different conditions. Hoyermann et al.[12] examined the reaction at a total pressure of about 4 Torr, finding a temperature dependence given by $5.6 \times 10^{-13} e^{855/T}$ cm^3 s^{-1}. Unfortunately the interpretation of this result is questionable since they omitted channel 1b. Sehested et al.[11] performed their experiments at 18 bar and over a range of 296−523 K arriving at a value of $(1.07 \pm 0.08) \times 10^{-11} e^{(46\pm27)/T}$ cm^3 s^{-1} for k_{r+o2}. Our results, near the high-pressure limit, give $k_{r+o2} = (3.1^{+1.0}_{-0.8}) \times 10^{-12} e^{(326\pm80)/T}$ cm^3 s^{-1}.

Measurements of $k_{ro2,0}/k_{prod,0}$ at 230, 295, and 350 K yield lower limits of 4.8×10^{-18}, 4.3×10^{-18}, and 2.9×10^{-18} cm^3, respectively. At a constant pressure, the branching fraction for channel 1b increases with increasing temperature. This is consistent with the $CH_3OCH_2 + O_2$ reaction proceeding through a $CH_3OCH_2O_2$* complex. As the temperature is raised, the extra available thermal energy enhances dissociation of the complex into the hydroxyl and formaldehyde products.

D. Atmospheric and Diesel Fuel Implications. Under atmospheric conditions the methoxymethyl radical behaves as a simple organic radical; namely, it adds oxygen to form the corresponding peroxy radical. The predominant removal pathway for this radical will likely involve its reaction with NO to produce CH_3OCH_2O. The latter molecule either reacts with O_2 or expels a hydrogen atom, in either case producing HO_2 and methylformate. The formaldehyde/OH channel is a minor one at pressures above 100 Torr. As the inset to Figure 14 shows, this remains true over the 230−350 K temperature range. Consequently the formation of formaldehyde from channel 1b during the atmospheric degradation of dimethyl ether should be of only minor importance.

This conclusion about the impact of the formaldehyde channel is predicated on the assumption that the methoxymethylperoxy radical is thermally stable. As the temperature is increased beyond 350 K toward combustion levels, reaction 1a will become reversible. When this happens, it will dramatically affect the net hydroxyl radical formation, even at "high" pressure, and, hence, the combustion of dimethyl ether. Instead of forming the relatively unreactive peroxy radical, the $CH_3OCH_2 + O_2$ reaction will form the more reactive hydroxyl radical, which will consume additional dimethyl ether, generate more heat, and, thereby, engender combustion. While this provides a plausible scenario for the high cetane number of dimethyl ether, additional experiments are needed to confirm the high-temperature behavior of reaction 1.

Conclusion

A detailed kinetic investigation of the chlorine-initiated oxidation of dimethyl ether has been presented. A combination of time-resolved UV spectroscopy and transient IR absorption techniques have been brought to bear on this problem. Recording the entire UV spectrum of the reaction mixture as a function of time allows us to disentangle contributions arising from the principal species of interest, CH_3OCH_2 and $CH_3OCH_2O_2$, as

well as those of potentially interfering contributions, such as molecular chlorine, dimethyl ether, and CH_3OCH_2Cl. Fitting the proposed reaction model to both concentration versus time profiles increases confidence in the reported rate constants.

One of the primary results is the direct detection of the hydroxyl radical and formaldehyde, thereby confirming a competition between addition and rearrangement/dissociation channels for the reaction between methoxymethyl radicals and molecular oxygen. This may begin to explain why dimethyl ether has good compression ignition characteristics, whereas other ethers are used as octane-enhancing fuel additives.

Acknowledgment. We thank E. W. Kaiser and T. J. Wallington for igniting our interest in the dimethyl ether study and for helpful discussions when the interpretation of experiments got a bit complicated.

References and Notes

(1) Leppard, W. R. *SAE Trans.* **1991**, 912313.
(2) Kapus, P. E.; Cartellieri, W. P. *SAE Trans.* **1995**, 952754.
(3) Sehested, J.; Møgelberg, T.; Wallington, T. J.; Kaiser, E. W.; Nielsen, O. J. *J. Phys. Chem.* **1996**, *100*, 17218.
(4) Maricq, M. M.; Szente, J. J. *J. Phys. Chem.* **1992**, *96*, 10862.
(5) Maricq, M. M.; Szente, J. J.; Kaiser, E. W. *J. Phys. Chem.* **1993**, *97*, 7970.
(6) Jenkin, M. E.; Hayman, G. D.; Wallington, T. J.; Hurley, M. D.; Ball, J. C.; Nielsen, O. J.; Ellermann, T. *J. Phys. Chem.* **1993**, *97*, 11712.
(7) Maricq, M. M.; Wallington, T. J. *J. Phys. Chem.* **1992**, *96*, 986.
(8) Mallard, W. G.; Westlely, F.; Herron, J. T.; Hampson, R. F. *NIST Chemical Kinetics Database Ver. 6.0*; NIST Standard Reference Data: Gaithersburg, MD, 1994.
(9) Langer, S.; Ljusgstrøm, E.; Ellermann, T.; Nielsen, O. J.; Sehested, J. *Chem. Phys. Lett.* **1995**, *240*, 53.
(10) Dagaut, P.; Wallington, T. J.; Kurylo, M. J. *J. Photochem. Photobiol.* **1989**, *48*, 187.
(11) Sehested, J.; Sehested, K.; Platz, J.; Egsgaard, H; Nielsen, O. J. *J. Phys. Chem.*, submitted.
(12) Hoyermann, K.; Nacke, F. *Twenty Sixth International Symposium on Combustion*; Napoli, July 1996.
(13) Timonen, R. S.; Gutman, D. *J. Phys. Chem.* **1986**, *90*, 2987.
(14) Masaki, A.; Tsunashima, S.; Washida, N. *J. Phys. Chem.* **1995**, *99*, 13126.